Progress of Theoretical Physics, Vol. 101, No. 5, May 1999

Relativistic and Non-Relativistic Mean Field Investigation of the Superdeformed Bands in ^{62}Zn

Hideki MADOKORO*) and Masayuki MATSUZAKI*, **)

Department of Physics, Kyushu University, Fukuoka 812-8581, Japan
and
Cyclotron Laboratory, The Institute of Physical and Chemical Research (RIKEN), Wako 351-0198, Japan
**Department of Physics, Fukuoka University of Education Munakata 811-4192, Japan*

(Received December 8, 1998)

Following the first discovery of the superdeformed (SD) band in the $A \sim 60$ mass region, we calculate several low-lying SD bands in ^{62}Zn using the relativistic mean field and Skyrme-Hartree-Fock models. Both models can reproduce the experimental moment of inertia very well, but we find that the calculated band, which corresponds to the experimentally observed band, does not become the lowest one. This trend is common among all the parameter sets which are widely used in RMF and SHF studies, and it seems to be connected with the fact that the position of the $g_{9/2}$ level is not reproduced in ^{56}Ni.

§1. Introduction

Recent developments in experimental techniques enable us to study nuclei with very large angular momenta. The study of superdeformed (SD) bands is one of the most interesting topics in such studies. The first experimental discovery was made for ^{152}Dy in 1986.[1] Since then, a large number of the SD bands have been observed in the $A \sim 130$, 150, 190 and 80 mass regions. These SD states are generated in the second minima in the potential energy surface which are connected with the deformed shell gaps such as $N, Z \sim 44$, 64, 86 and 116. Based on a theoretical calculation indicating that there exist the $N, Z \sim 30$ shell gaps, the SD bands in the $A \sim 60$ mass region were also predicted.[2] In spite of much experimental efforts, however, such SD states had not been observed due to some experimental difficulties. In 1997, a cascade of six γ rays forming a new band was observed in ^{62}Zn.[3] This was the first experimental discovery of the SD bands in this mass region. The extracted rotational frequency, $\Omega \simeq 1.0$–1.6 MeV, is the highest among those observed to this time. In addition, there are several interesting features in this mass region. For example, the valence neutrons and protons occupy the same orbits, in contrast with the situation in other mass regions, and the residual neutron-proton pairing at high spin may be observed. Another example is the decay of these SD states via proton emission due to a very low Coulomb barrier. Such a decay of well-deformed high spin states has already been observed in ^{58}Cu.[4] Because of the simpleness of the

*) E-mail: madokoro@postman.riken.go.jp
**) E-mail: matsuza@fukuoka-edu.ac.jp

level structure near the Fermi surface, systematic studies can be easily done in this mass region, where only the $N_{\rm osc} = 3$ and 4 orbits are relevant. Several groups have already started such work.[5)-7)]

In this paper, we apply the relativistic mean field (RMF) model to the SD bands in ^{62}Zn. The RMF model is now considered as a reliable method similar to the non-relativistic Hartree-Fock model to describe various properties of finite nuclei, not only β-stable but also β-unstable nuclei. Since the work of Walecka and his collaborators,[8)] the RMF model has been applied to nuclear matter and the ground states of finite nuclei with great success, as well as to Dirac phenomenology for scattering data. Some groups have also attempted to apply this model to the excited states in finite nuclei. In 1989, the Munich group made a first attempt to describe the properties of rotating nuclei.[9)] They applied this model mainly to SD bands in several mass regions.[10)-12),7)] Because the RMF model is currently under refinement, it is important to apply this model to as wide a variety of nuclear phenomena as possible, and to check its applicability further. We believe that the application of this model to the SD bands in ^{62}Zn will serve such a purpose. For comparison, we also calculate the same SD bands using the Skyrme-Hartree-Fock (SHF) model. The RMF and SHF models give very similar results in the low spin region. We expect that there may be different observed results for these two models when applied to very high spin states in neutron-deficient unstable nuclei. Preliminary results of this paper have been previously reported.[5)]

§2. Formulation

The starting point of the RMF model is the following Lagrangian, which contains the nucleon and several kinds of meson fields, such as σ-, ω- and ρ-mesons, together with the photon fields (denoted by A) mediating the Coulomb interaction:

$$\mathcal{L} = \mathcal{L}_N + \mathcal{L}_\sigma + \mathcal{L}_\omega + \mathcal{L}_\rho + \mathcal{L}_A + \mathcal{L}_{\rm int} + \mathcal{L}_{{\rm NL}\sigma} + \mathcal{L}_{{\rm NL}\omega},$$

$$\begin{aligned}
\mathcal{L}_N &= \overline{\psi}(i\gamma^\alpha\partial_\alpha - M)\psi, \\
\mathcal{L}_\sigma &= \frac{1}{2}(\partial_\alpha\sigma)(\partial^\alpha\sigma) - \frac{1}{2}m_\sigma^2\sigma^2, \\
\mathcal{L}_\omega &= -\frac{1}{4}\Omega_{\alpha\beta}\Omega^{\alpha\beta} + \frac{1}{2}m_\omega^2\omega_\alpha\omega^\alpha, \\
\mathcal{L}_\rho &= -\frac{1}{4}\vec{R}_{\alpha\beta}\cdot\vec{R}^{\alpha\beta} + \frac{1}{2}m_\rho^2\vec{\rho}_\alpha\cdot\vec{\rho}^\alpha, \\
\mathcal{L}_A &= -\frac{1}{4}F_{\alpha\beta}F^{\alpha\beta}.
\end{aligned}$$

Here,

$$\begin{aligned}
\Omega_{\alpha\beta} &= \partial_\alpha\omega_\beta - \partial_\beta\omega_\alpha, \\
\vec{R}_{\alpha\beta} &= \partial_\alpha\vec{\rho}_\beta - \partial_\beta\vec{\rho}_\alpha - g_\rho\vec{\rho}_\alpha\times\vec{\rho}_\beta, \\
F_{\alpha\beta} &= \partial_\alpha A_\beta - \partial_\beta A_\alpha,
\end{aligned}$$

are the field strength tensors. $\mathcal{L}_{\rm int}$ is the interaction part between nucleons and mesons:

$$\begin{aligned}\mathcal{L}_{\rm int} &= g_\sigma \overline{\psi}\psi\sigma - g_\omega \overline{\psi}\gamma^\alpha\psi\omega_\alpha \\ &\quad -g_\rho\overline{\psi}\gamma^\alpha\overrightarrow{\tau}\psi\cdot\overrightarrow{\rho}_\alpha - e\overline{\psi}\gamma^\alpha\frac{1-\tau_3}{2}\psi A_\alpha.\end{aligned}$$

In the standard applications, non-linear self-interactions among the σ-mesons,

$$\mathcal{L}_{{\rm NL}\sigma} = \frac{1}{3}g_2\sigma^3 - \frac{1}{4}g_3\sigma^4,$$

are also included. These are crucial for realistic descriptions of deformed nuclei. We also include the quartic term of the ω-mesons,

$$\mathcal{L}_{{\rm NL}\omega} = \frac{1}{4}c_3(\omega^\alpha\omega_\alpha)^2.$$

Applying the variational principle to the Lagrangian gives the equations of motion. Within the mean field approximation, these are the Dirac equation for single nucleon fields ψ_i and the Klein-Gordon equations for the classical meson and photon fields. After solving these equations, we can calculate various properties of finite nuclei.

For application to rotating nuclei within the cranking assumption, it is necessary to write the Lagrangian in a uniformly rotating frame which rotates around the x-axis with a constant angular velocity Ω, from which the equations of motion in this frame can be obtained. Because the rotating frame is not an inertial frame, a fully covariant formulation is desirable, and we obtain this using the technique of general relativity known as tetrad formalism.[13] The procedure is as follows. First, according to tetrad formalism, we can write the Lagrangian in the non-inertial frame represented by the metric tensor $g_{\mu\nu}(x)$. Then the variational principle gives the equations of motion in this non-inertial frame. Finally, substituting the metric tensor of the uniformly rotating frame,

$$g_{\mu\nu}(x) = \begin{pmatrix} 1-\Omega^2(y^2+z^2) & 0 & \Omega z & -\Omega y \\ 0 & -1 & 0 & 0 \\ \Omega z & 0 & -1 & 0 \\ -\Omega y & 0 & 0 & -1 \end{pmatrix},$$

leads to the desired equations of motion. The resulting equations are

$$\begin{aligned}\left\{\boldsymbol{\alpha}\cdot\left(\frac{1}{i}\boldsymbol{\nabla} - g_\omega\boldsymbol{\omega}(x)\right) + \beta(M - g_\sigma\sigma(x))\right. \\ \left. + g_\omega\omega^0(x) - \Omega(L_x+\Sigma_x)\right\}\psi_i(x) = \epsilon_i\psi_i(x),\end{aligned}$$

$$\left\{-\boldsymbol{\nabla}^2 + m_\sigma^2 - \Omega^2L_x^2\right\}\sigma(x) - g_2\sigma^2(x) + g_3\sigma^3(x) = g_\sigma\rho_s(x),$$

$$\left\{-\boldsymbol{\nabla}^2 + m_\omega^2 - \Omega^2L_x^2\right\}\omega^0(x) - c_3\{(\omega^0(x))^2 - (\boldsymbol{\omega}(x))^2\}\omega^0(x) = g_\omega\rho_v(x),$$

$$\left\{-\boldsymbol{\nabla}^2 + m_\omega^2 - \Omega^2(L_x+S_x)^2\right\}\boldsymbol{\omega}(x) - c_3\{(\omega^0(x))^2 - (\boldsymbol{\omega}(x))^2\}\boldsymbol{\omega}(x) = g_\omega\boldsymbol{j}_v(x),$$

where the ρ-meson and photon fields are omitted for simplicity, although they are included in the numerical calculation. These equations are the same as those obtained by the Munich group. (For details, see Ref. 14).)

§3. Numerical results

The equations appearing at the end of the previous section can be solved by the standard iterative diagonalization method using the three-dimensional harmonic oscillator eigenfunctions. Because our method of numerical calculation is essentially the same as that of the Munich group[15] and its details are given in Ref. 16), we here give only the model parameters used. The cutoff parameters for the nucleon and meson fields are taken to be $N_{\rm F} = 10$ and $N_{\rm B} = 10$, respectively. When we adopt larger cutoffs, $N_{\rm F} = N_{\rm B} = 12$, it is found that the results change by 0.01% for the total energies, 1.0–1.5% for dynamical moments of inertia, and 3–4% for quadrupole moments. These small errors do not affect our conclusion. The parameter sets NL1,[17] NL3,[18] NL-SH[19] and TM1[20] are adopted. The first three sets contain only the non-linear σ terms, while the ω^4 term is also included in TM1.

Figure 1 displays the single neutron Routhians of the lowest SD configuration in ^{60}Zn, which are calculated using the parameter set TM1. There appears a well-

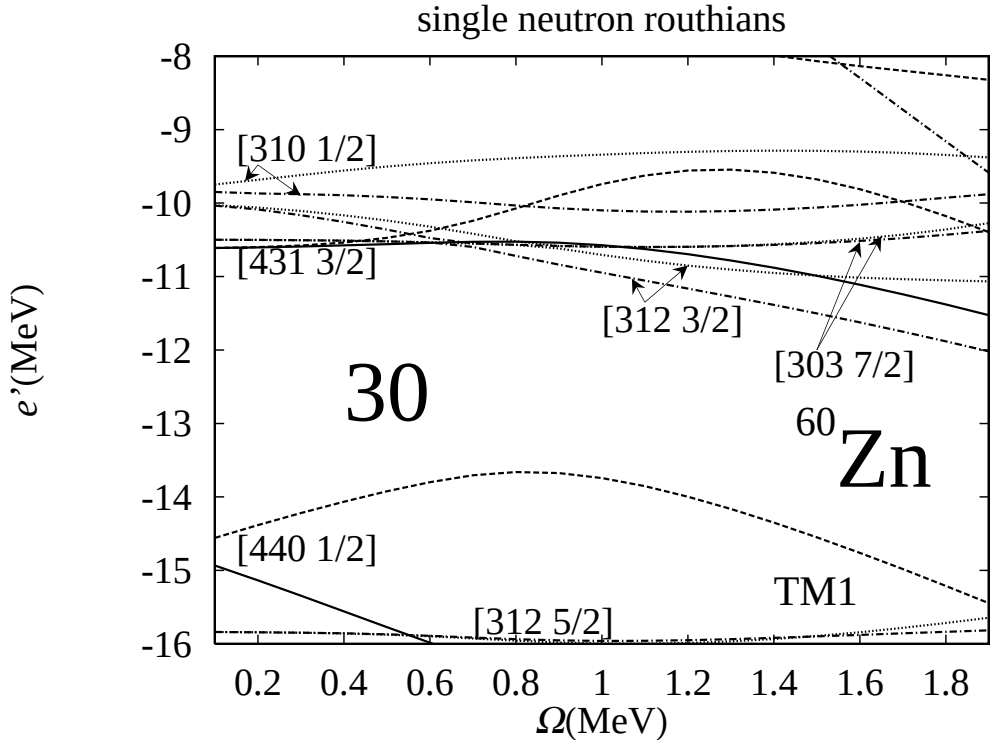

Fig. 1. The single neutron Routhians in the lowest SD band in ^{60}Zn calculated using the set TM1. Dashed, solid, dot-dashed and dotted lines represent $(\pi = +, r = +i)$, $(\pi = +, r = -i)$, $(\pi = -, r = +i)$ and $(\pi = -, r = -i)$ orbits, respectively.

developed $N = 30$ gap as the [440 1/2] ($r = +i$) orbit is strongly down-sloping with respect to the rotational frequency in the high spin part. All the SD states in this mass region can be represented as particle-hole excited states on top of this ^{60}Zn configuration. The SD configurations of ^{62}Zn are symbolically denoted as $\pi 4^{N_\mathrm{p}}$ and $\nu 4^{N_\mathrm{n}}$, which mean that N_p protons and N_n neutrons occupy the $N = 4$ ($g_{9/2}$) orbits. According to Ref. 3), the proton configurations are fixed to $N_\mathrm{p} = 2$. Different SD bands are then formed, depending on the number of neutrons lifted into the $N_\mathrm{osc} = 4$ orbits, which is taken as $N_\mathrm{n} = 2$–4 in this work. We consider the SD configurations A: $\pi 4^2 \nu 4^2$, D: $\pi 4^2 \nu 4^3$ and C: $\pi 4^2 \nu 4^4$. Here, different configurations are possible for D according to the parity-signature quantum numbers ($\pi = \pm, r = \pm i$) of the last two nucleons. The occupation numbers in each parity-signature block for these configurations are explicitly written as

$$\begin{aligned}
&\mathrm{A}: \pi[8++;8+-;7-+;7--]\nu[8++;8+-;8-+;8--](\pi_\mathrm{tot} = +, r_\mathrm{tot} = +1),\\
&\mathrm{D1}: \pi[8++;8+-;7-+;7--]\nu[8++;9+-;8-+;7--](\pi_\mathrm{tot} = -, r_\mathrm{tot} = +1),\\
&\mathrm{D2}: \pi[8++;8+-;7-+;7--]\nu[8++;9+-;7-+;8--](\pi_\mathrm{tot} = -, r_\mathrm{tot} = -1),\\
&\mathrm{D3}: \pi[8++;8+-;7-+;7--]\nu[9++;8+-;8-+;7--](\pi_\mathrm{tot} = -, r_\mathrm{tot} = -1),\\
&\mathrm{D4}: \pi[8++;8+-;7-+;7--]\nu[9++;8+-;7-+;8--](\pi_\mathrm{tot} = -, r_\mathrm{tot} = +1),\\
&\mathrm{C}: \pi[8++;8+-;7-+;7--]\nu[9++;9+-;7-+;7--](\pi_\mathrm{tot} = +, r_\mathrm{tot} = +1),
\end{aligned}$$

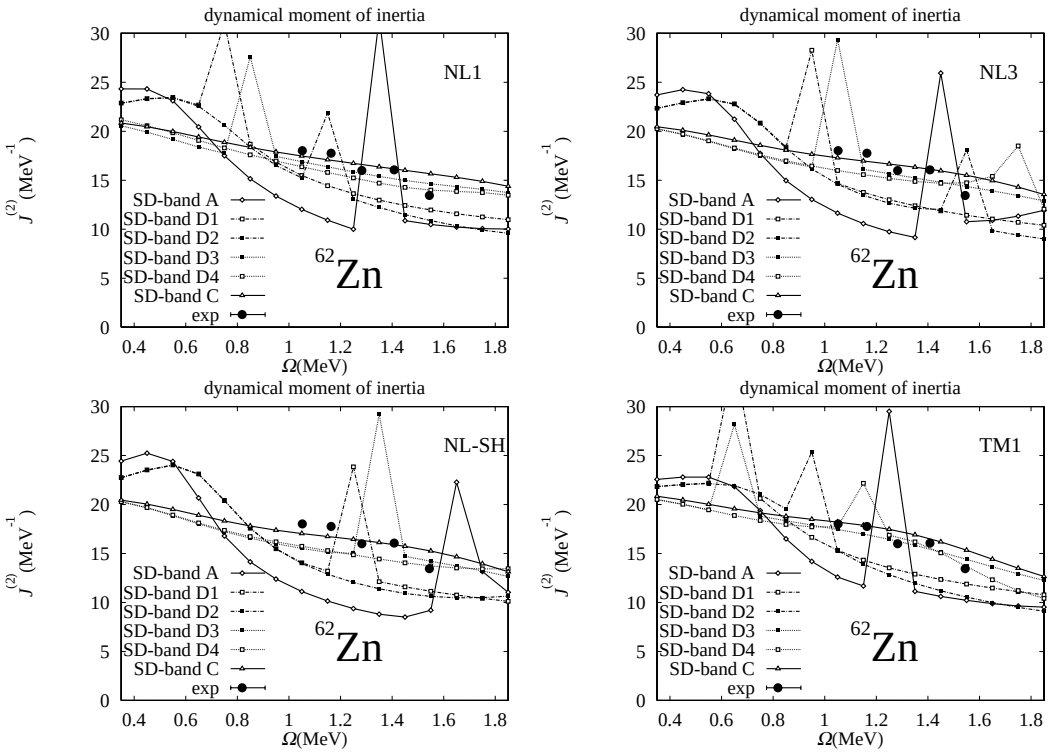

Fig. 2. The calculated and experimental dynamical moments of inertia. The calculations were done using the RMF parameter sets NL1, NL3, NL-SH and TM1.

where the total parities and signatures are also shown. Figure 2 gives the calculated dynamical moments of inertia,

$$J^{(2)} = \left(\frac{d^2E}{dJ_x^2}\right)^{-1} = \frac{dJ_x}{d\Omega},$$
$$J_x(\Omega) = \sum_i \langle j_x \rangle_i = \sqrt{I(I+1)},$$

of several SD bands in ^{62}Zn. The experimental data are also given in the same figure. Several jumps are caused by the crossing between the [303 7/2] neutron orbits and the [312 3/2] orbits (or the [310 1/2] ones). Apart from these crossings, the bands D3, D4 and C seem to reproduce the experimental values well for all the parameter sets. Figures 3 and 4 display the effective alignment of each band with respect to the lowest SD band in ^{60}Zn. The effective alignment of band 1 with respect to band 2 is defined as

$$i_{\rm eff}(\Omega) = I_1(\Omega) - I_2(\Omega),$$

which thus represents the contributions to the total spin coming from additional particles. This quantity is widely used to assign configurations of SD bands whose spins are not determined experimentally.[21),12)] We choose the lowest SD band in ^{60}Zn as a reference which has recently been reported and whose spin and parity

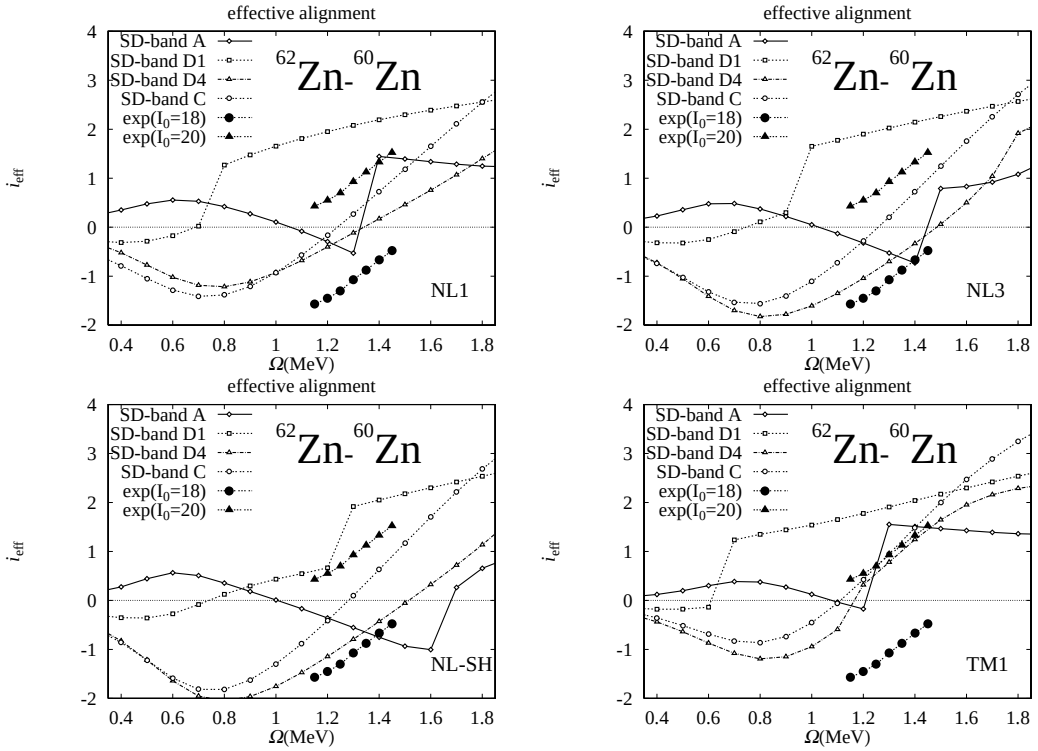

Fig. 3. The effective alignments of the bands which have positive signatures ($I = 0, 2, 4, \cdots$).

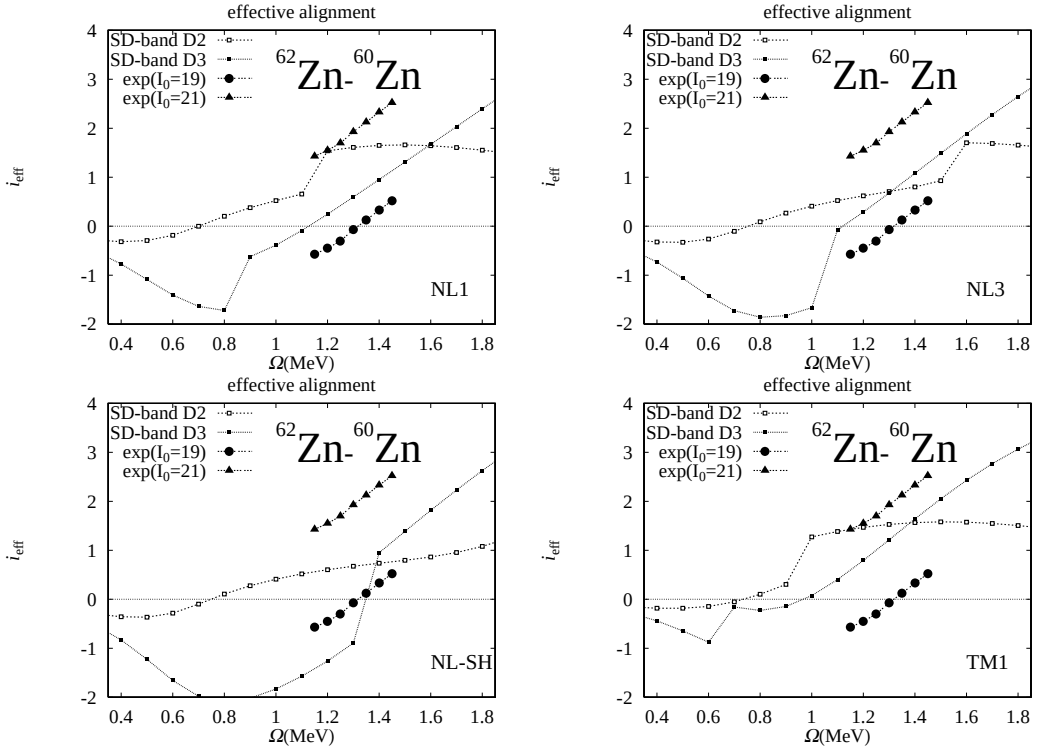

Fig. 4. The effective alignments of the bands which have negative signatures ($I = 1, 3, 5, \cdots$).

are already known.[22),7)] In contrast to ^{60}Zn, no spin and parity assignment has been made for any SD bands in ^{62}Zn, and thus we assume that the lowest transition observed corresponds to that from I_0 to $I_0 - 2$. The values of I_0 are shown in the figures. We can see small but clear differences depending on the parameter set used. In the case of NL1, the band C gives a good result with the assumption $I_0 = 20$, while the band D3 is also good if I_0 is assumed to be 19, although in both cases there are deviations from the experimental values. If NL3 or NL-SH is adopted, the band D4 becomes the best one, with $I_0 = 18$ (the band C is also not so bad). Finally, the bands D4 and C reproduce the experimental values very well when TM1 is used, assuming that I_0 is 20. As a whole, the bands D4 and C give good results; at least the behavior of the experimental values as functions of the rotational frequency is well reproduced.

Figure 5 displays the quadrupole deformations. The experimentally extracted value is shown with an error bar. Although this appears at $\Omega = 1.25$ MeV, we should keep in mind that this is a value averaged over some range of spins. The bands D reproduce the experimental value very well, although the band C is also within the error bar. The band A gives values that are somewhat too small in all the parameter sets. From these results, we can conclude that the experimentally observed one will correspond to the band D4 or C in our calculation, although the former implies a difficulty that it contains one neutron that exists not in the favored ($r = +i$) but in the unfavored ($r = -i$) [431 3/2] orbit (see Fig. 1). Because

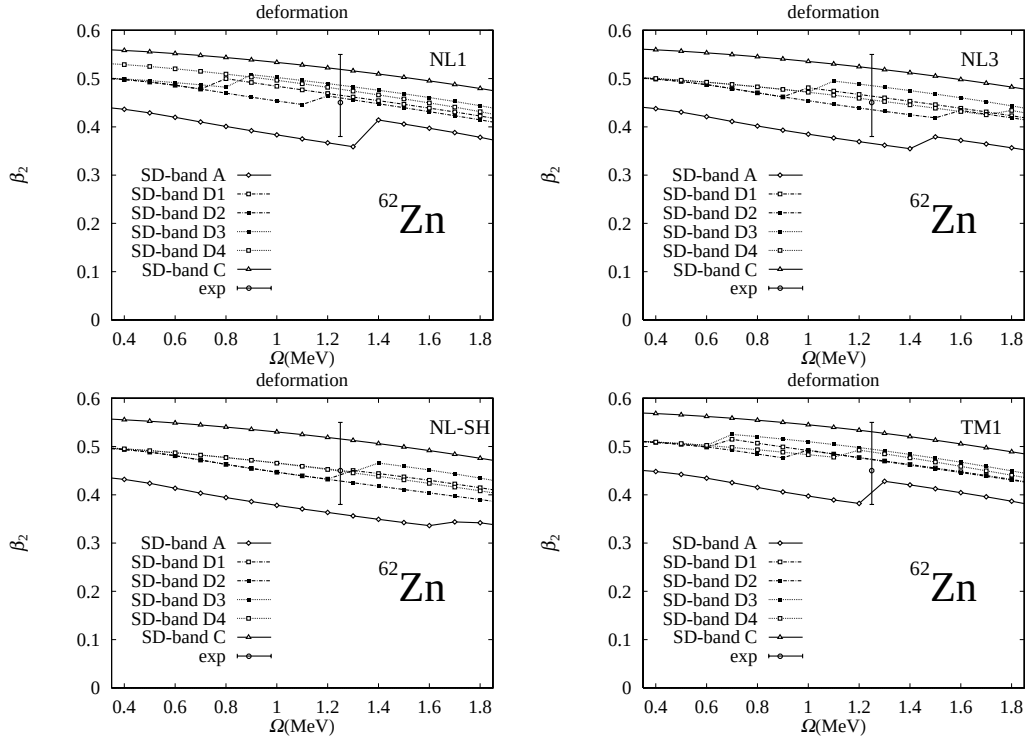

Fig. 5. The calculated and experimental quadrupole deformations.

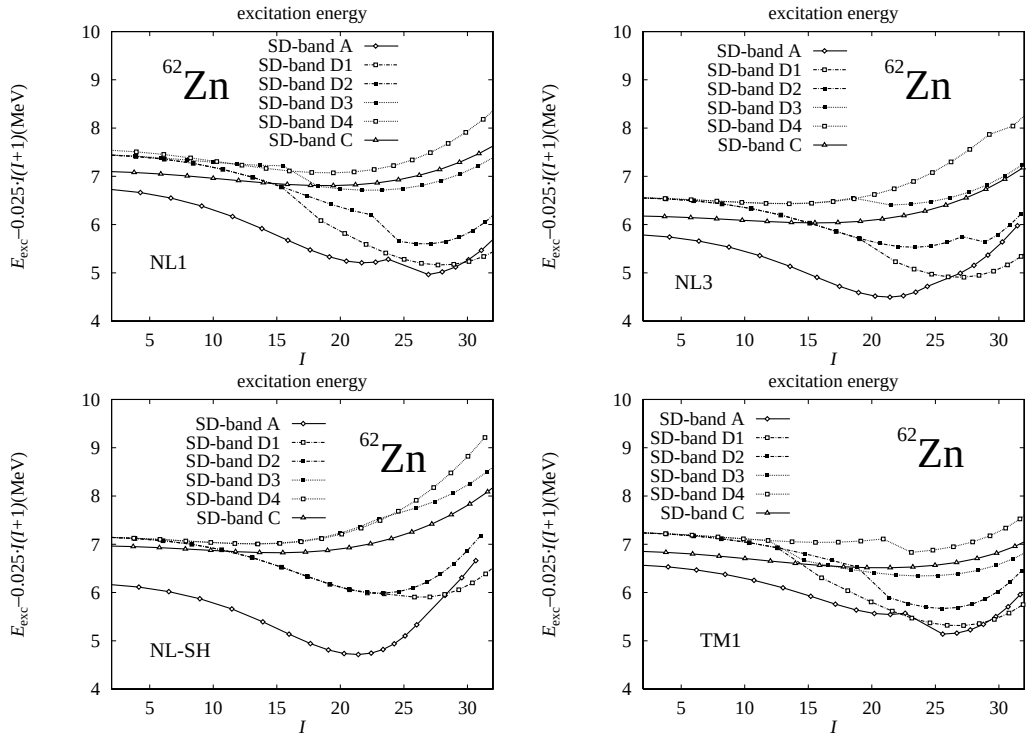

Fig. 6. The calculated total Routhians with respect to a rigid rotor reference.

these two have the same signature but different parities ($I^\pi = 0^-, 2^-, 4^-, \cdots$ for the band D4, $I^\pi = 0^+, 2^+, 4^+, \cdots$ for the band C), we can determine which configuration corresponds to the observed one after its spin and parity are assigned. The excitation energies of the bands mentioned above are shown in Fig. 6 relative to a rigid rotor reference. The bands D4 and C which give the best result are located more than 1 MeV higher than the lowest band in all the parameter sets. This result is consistent with that of the configuration-dependent shell correction approach given in Refs. 3) and 23).

For comparison, we also performed the SHF calculation for the same bands in ^{62}Zn, using the code HFODD (ver. 1.75), which was developed by Dobaczewski and Dudek.[24] The parameter sets SIII,[25] SkM*,[26] SkP[27] and SLy4[28] were adopted. In some cases when using the sets SIII, SkM* and SkP, well-converged solutions for given SD configurations are not obtained, especially for the bands A, D2 and D4. This may arise from the energetic competition between the [303 7/2] orbits and the [312 3/2] (or [310 1/2]) orbits. In these cases, we derive only the well-converged solutions. Figure 7 displays the single neutron Routhians of the lowest SD configuration in ^{60}Zn using the parameter set SLy4. We can see a well-developed $N = 30$ gap, similar to the case depicted in Fig. 1. Figures 8–12 display the calculated moments of inertia, the effective alignments, the quadrupole deformations and the excitation energies of the same SD bands as the RMF calculation. In Fig. 8, we can

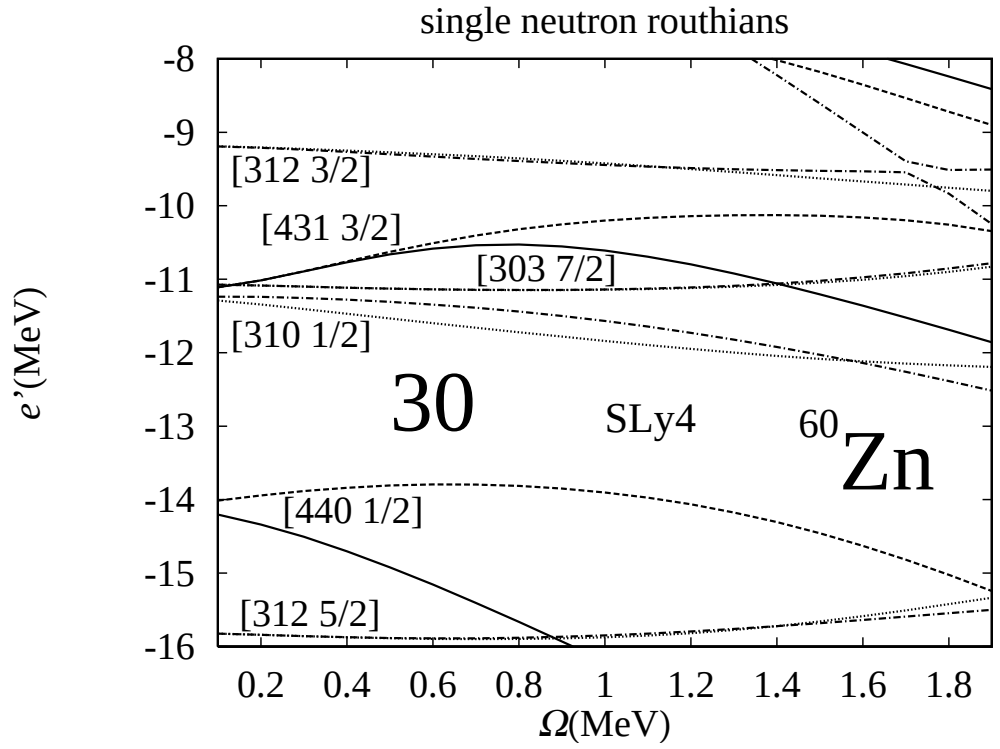

Fig. 7. The single neutron Routhians in the lowest SD band in ^{60}Zn calculated using the set SLy4. The meaning of each line is the same as in Fig. 1.

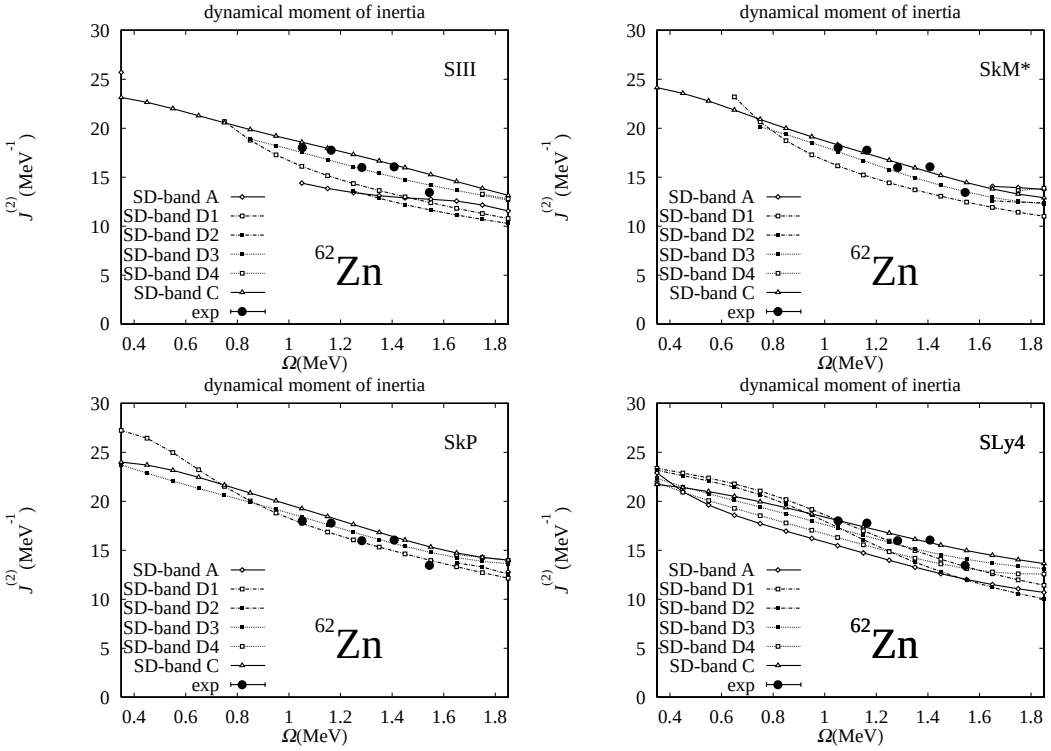

Fig. 8. The calculated and experimental dynamical moments of inertia. The calculations were done using the SHF parameter sets SIII, SkM*, SkP and SLy4. For the band C, the same result using the set SLy4 is given in Fig. 3 of Ref. 30).

see that the band D3 gives the best result for all the sets. The band C is also good in the case of SkM* and SLy4, while the calculated values of the band C are slightly large compared with the experimental value for SIII and SkP. In the case of SLy4, the band D1 is also good.

As for the quadrupole deformations, the bands D as well as the band A can reproduce the experimental value, although the band C is also within the error bar (see Fig. 11). From the analysis of the effective alignments, the band C reproduces the experimental value quite well in all the sets (see Figs. 9 and 10). Thus the SHF calculations strongly suggest that the band C is the best candidate for the experimentally observed one. As in the RMF calculation, this band is again located more than 1 MeV higher than the lowest band, as can be seen in Fig. 12. Our group first pointed out that the calculated moment of inertia of the lowest SD configuration in ^{62}Zn does not reproduce the experimental value.[5] The possible reason for this is that the position of the $g_{9/2}$ orbit may be unexpectedly high, as stated in Ref. 7). To see this, we calculated the single neutron levels in the ground state of the doubly magic ^{56}Ni nucleus. The results are shown in Fig. 13. The experimental levels are taken from the data of the low-lying states in ^{55}Ni and ^{57}Ni. Although these data do not precisely represent the 'bare' single particle levels, in which the effects of the coupling between the outside particle and the low-lying collective mode of the core

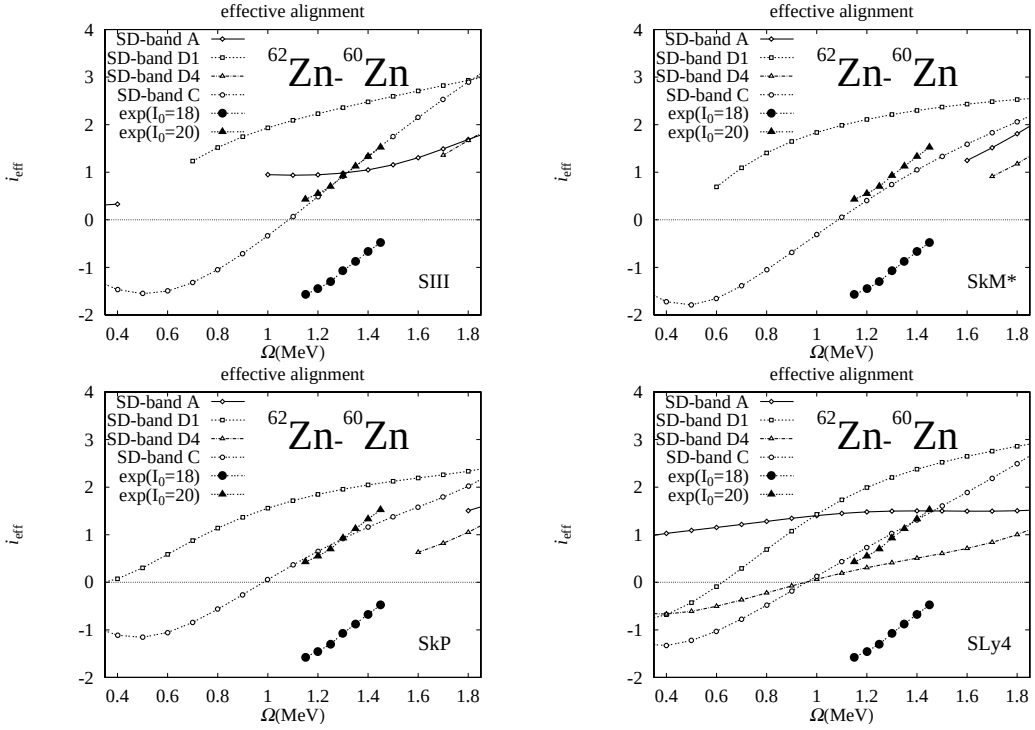

Fig. 9. The effective alignments of the bands which have positive signatures ($I = 0, 2, 4, \cdots$).

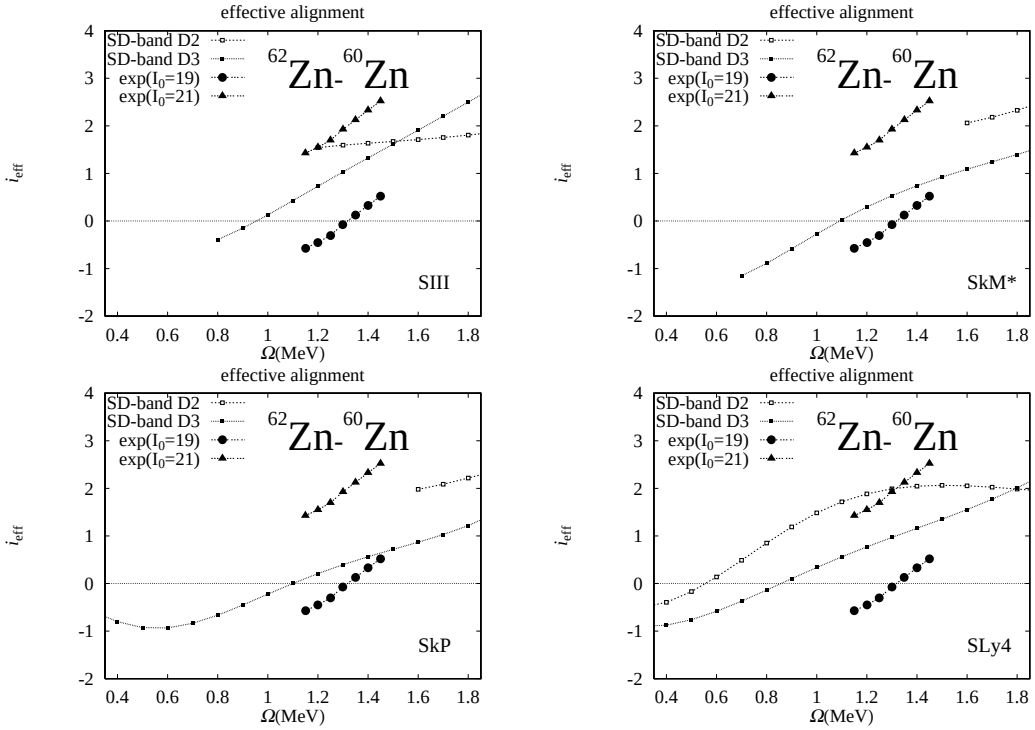

Fig. 10. The effective alignments of the bands which have negative signatures ($I = 1, 3, 5, \cdots$).

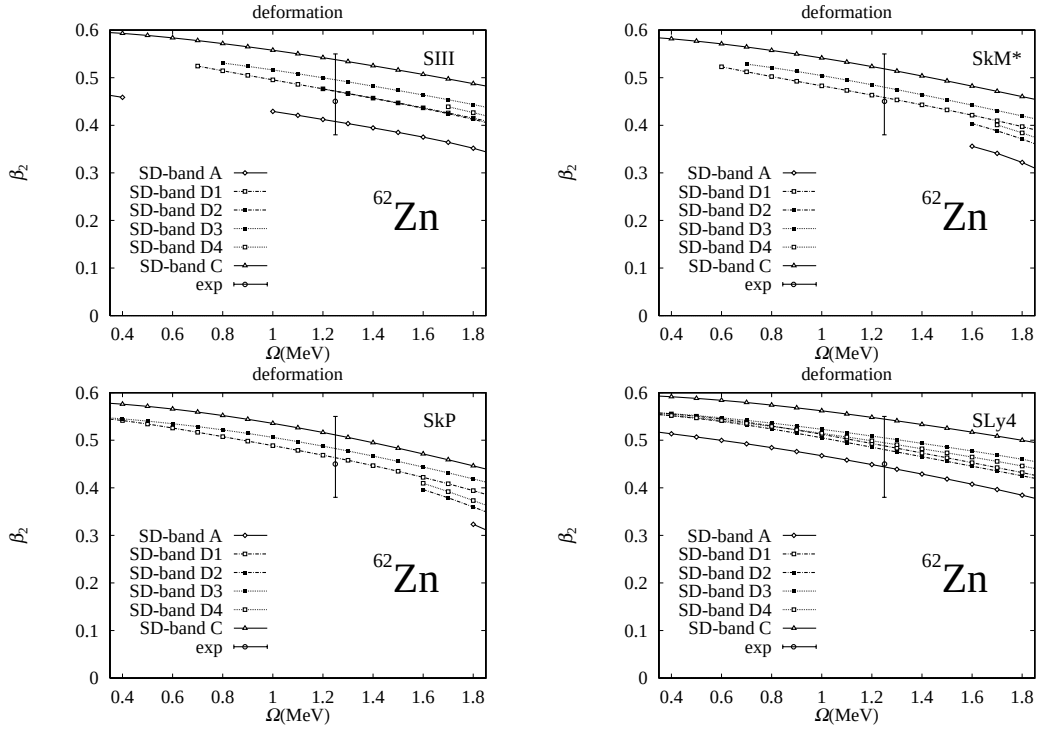

Fig. 11. The calculated and experimental quadrupole deformations.

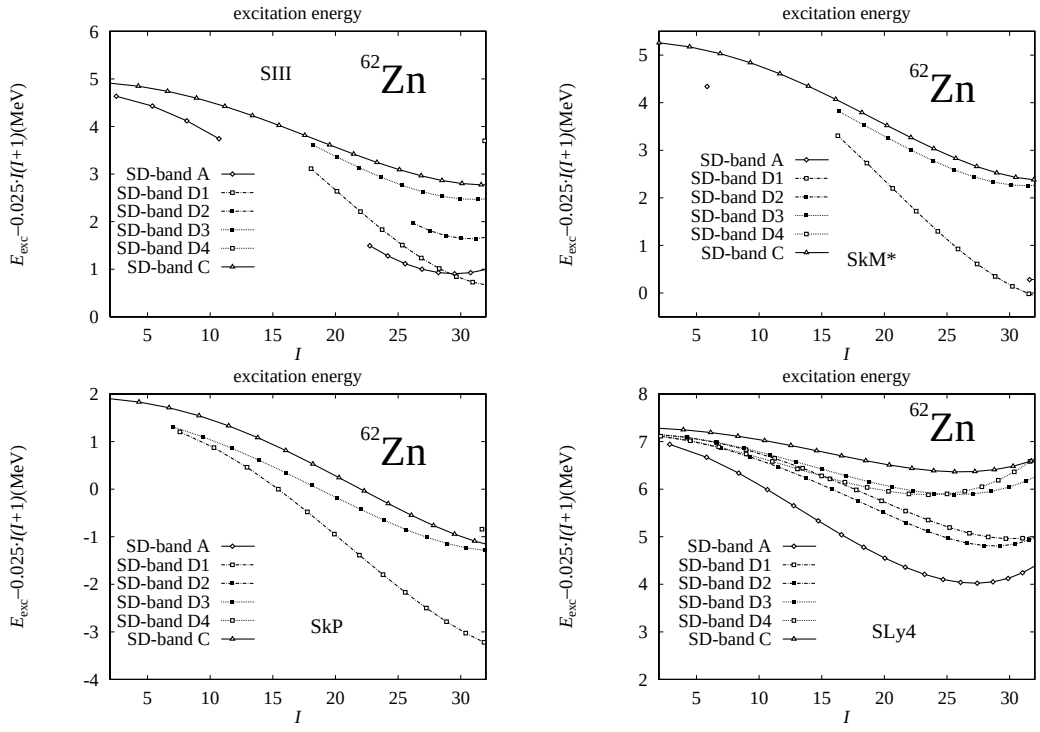

Fig. 12. The calculated total Routhians with respect to a rigid rotor reference.

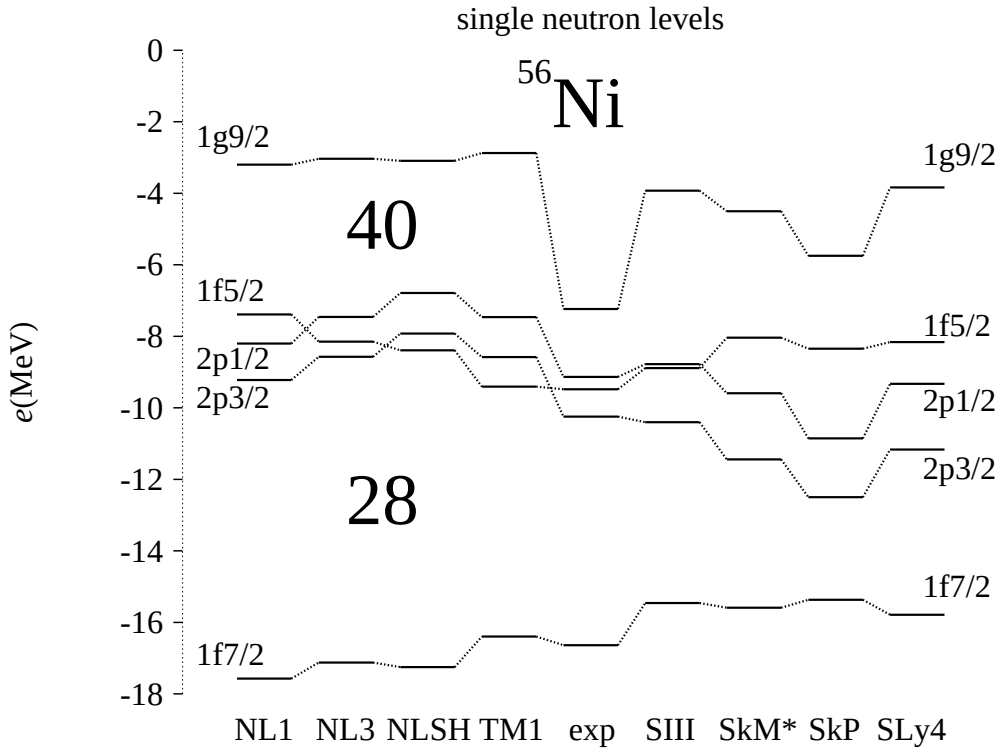

Fig. 13. The single neutron levels in the ground state of a doubly magic ^{56}Ni nucleus. The experimental values are extracted from those of the low-lying excited states in ^{55}Ni and ^{57}Ni.

are carefully subtracted,[29] we believe the deviations from these 'bare' single particle energies are not large. This can be confirmed at least for the pf orbits, where the differences are only 0.2–0.3 MeV.[29] At a glance we can see that the experimental position of the $g_{9/2}$ orbit is significantly lower than those of theoretical calculations. This trend is common among all the parameter sets which are investigated in this work. If the position of the $g_{9/2}$ orbit is too high, the bands which contain 3 or 4 neutrons in the $N_{\rm osc} = 4$ orbits (for example, the bands D4 and C) will attain very high positions compared with the bands which contain only 2 neutrons in the $N_{\rm osc} = 4$ orbits (for example, the band A). To this time, no one has given a definite explanation for this puzzle.

§4. Summary

We have studied the SD bands in ^{62}Zn using the RMF model, including a recently discovered band. For comparison, we also performed SHF calculations for the same SD bands in this nucleus. The two models give similar results as a whole. Looking at them closely, however, for the RMF calculations, the bands D4 and C give the best results in all the examined parameter sets. The SHF calculations, on the other hand, strongly suggest that the band C corresponds to the experimental data. When looking at the excitation energies, we confront a puzzling problem: the bands D4

and C, which seem to correspond to the experimentally observed band, are located more than 1 MeV higher than the lowest one. This result is common in both the RMF and SHF investigations. This may indicate the incorrect position of the single neutron $g_{9/2}$ orbit. To determine whether this is true or not, we calculated the single neutron levels in ^{56}Ni. The result implies that the calculated positions of the $g_{9/2}$ orbit are significantly higher than that of the experimentally derived one. In addition, our preliminary calculation [31] of the SD bands in ^{61}Zn shows a trend quite similar to that in ^{62}Zn; that is, the band which is considered to be a candidate for the experimental data does not become the lowest one. These facts support the discussion above. Clearly it is necessary to examine other isotopes in this mass region in order to see whether the position of the $g_{9/2}$ orbit is correctly reproduced or not in these neutron-deficient nuclei. Recently, a number of new SD and largely deformed (LD) bands in the $_{28}$Ni, $_{29}$Cu and $_{30}$Zn isotopes have been observed and reported. [32),33)] This makes it possible to perform systematic comparisons between calculated and experimental values. Such a work is now under progress and will appear in a forthcoming paper.

Acknowledgements

One of the authors (H. M.) would like to acknowledge the Junior Research Associate Program of the Japan Science and Technology Agency. Some of the numerical calculations in this work were done using the computer systems of the Research Center for Nuclear Physics (RCNP), Osaka University.

References

1) P. J. Twin et al., Phys. Rev. Lett. **57** (1986), 811.
2) I. Ragnarsson, *Proc. of the Workshop on the Science of Intense Radioactive Ion Beams, Los Alamos, April 10-12, 1990*, p. 199.
3) C. E. Svensson et al., Phys. Rev. Lett. **79** (1997), 1233.
4) D. Rudolph et al., Phys. Rev. Lett. **80** (1998), 3018.
5) H. Madokoro and M. Matsuzaki, *Proc. of the XVII RCNP Intern. Symp. on Innovative Computational Methods in Nuclear Many-Body Problems, Osaka, 1997*, ed. H. Horiuchi et al. (World Scientific, Singapore, 1998), p. 366.
6) J. Dobaczewski, Preprint nucl-th/9811043 (1998).
7) A. V. Afanasjev, I. Ragnarsson and P. Ring, Preprint nucl-th/9809074 (1998).
8) S. A. Chin and J. D. Walecka, Phys. Lett. **B52** (1974), 24.
J. D. Walecka, Ann. of Phys. **83** (1974), 491.
S. A. Chin, Ann. of Phys. **108** (1977), 301.
9) W. Koepf and P. Ring, Nucl. Phys. **A493** (1989), 61; **A511** (1990), 279.
10) J. König and P. Ring, Phys. Rev. Lett. **71** (1993), 3079.
A. V. Afanasjev, J. König and P. Ring, Phys. Lett. **B367** (1996), 11.
J. König, Ph. D. thesis (1996), unpublished.
11) A. V. Afanasjev, J. König and P. Ring, Nucl. Phys. **A608** (1996), 107.
12) A. V. Afanasjev, G. A. Lalazissis and P. Ring, Nucl. Phys. **A634** (1998), 395.
13) S. Weinberg, *Gravitation and Cosmology: Principles and Applications of The General Theory of Relativity* (John Willy and Sons, New York, 1972), p. 365.
N. D. Birrell and P. C. W. Davies, *Quantum Fields in Curved Space* (Cambridge Univ. Press, London, 1982), p. 81.
14) H. Madokoro and M. Matsuzaki, Phys. Rev. **C56** (1997), R2934.
15) J. König, private communication (1996).

16) Y. K. Gambhir, P. Ring and A. Thimet, Ann. of Phys. **198** (1990), 132.
17) P.-G. Reinhard, M. Rufa, J. Maruhn, W. Greiner and J. Friedrich, Z. Phys. **A323** (1986), 13.
18) G. A. Lalazissis, J. König and P. Ring, Phys. Rev. **C55** (1997), 540.
19) M. M. Sharma, M. A. Nagarajan and P. Ring, Phys. Lett. **B312** (1993), 377.
20) Y. Sugahara and H. Toki, Nucl. Phys. **A579** (1994), 557.
21) I. Ragnarsson, Phys. Lett. **B264** (1991), 5; Nucl. Phys. **A557** (1993), 167c.
22) C. E. Svensson et al., *Abstract of Nuclear Structure '98, Gatlinburg, Tennessee, USA, August 10-15, 1998*, p. 130.
23) C. E. Svensson et al., Phys. Rev. Lett. **80** (1998), 2558.
24) J. Dobaczewski and J. Dudek, Comp. Phys. Commun. **102** (1997), 166, 183.
J. Dobaczewski, Preprint nucl-th/9801056 (1998); private communication (1998).
25) M. Beiner, H. Flocard, Nguyen Van Giai and P. Quentin, Nucl. Phys. **A238** (1975), 29.
26) J. Bartel, P. Quentin, M. Brack, C. Guet and H.-B. Håkansson, Nucl. Phys. **A386** (1982), 79.
27) J. Dobaczewski, H. Flocard and J. Treiner, Nucl. Phys. **A422** (1984), 103.
28) E. Chabanat et al., Physica Scripta **T56** (1995), 231.
29) L. Trache et al., Phys. Rev. **C54** (1996), 2361.
30) D. Rudolph et al., Nucl. Phys. **A630** (1998), 417c.
31) H. Madokoro and M. Matsuzaki, in preparation.
32) C.-H. Yu et al., *Abstract of Nuclear Structure '98, Gatlinburg, Tennessee, USA, August 10-15, 1998*, p. 155.
33) W. Nazarewicz, private communication (1998).